01 Feb 2022

Impact of Clay Stabilizer on the Methane Desorption Kinetics and Isotherms of Longmaxi Shale, China

Zhong Hua Liu

Jia Chun Wang

Baojun Bai
Missouri University of Science and Technology, baib@mst.edu

Yan Ling Wang

Recommended Citation

Z. H. Liu et al., "Impact of Clay Stabilizer on the Methane Desorption Kinetics and Isotherms of Longmaxi Shale, China," *Petroleum Science*, vol. 19, no. 1, pp. 234 - 244, KeAi Communications, Feb 2022.
The definitive version is available at https://doi.org/10.1016/j.petsci.2021.09.025

Petroleum Science 19 (2022) 234–244

Contents lists available at ScienceDirect

Petroleum Science

journal homepage: www.keaipublishing.com/en/journals/petroleum-science

Original Paper

Impact of clay stabilizer on the methane desorption kinetics and isotherms of Longmaxi Shale, China

Zhong-Hua Liu [a, d], Jia-Chun Wang [b], Bao-Jun Bai [c, *], Yan-Ling Wang [a, **]

[a] School of Petroleum Engineering, China University of Petroleum (East China), Qingdao, 266580, Shandong, China
[b] Exploration and Development Research Institute of Daqing Oilfield Co Ltd., Daqing, 163712, Heilongjiang, China
[c] Geosciences and Geological and Petroleum Engineering, Missouri University of Science and Technology, Rolla, MO, 65409, USA
[d] School of Petroleum and Natural Gas Engineering, Chongqing University of Science and Technology, Chongqing, 401332, China

ARTICLE INFO

Article history:
Received 4 March 2021
Accepted 13 August 2021
Available online 23 September 2021

Edited by Yan-Hua Sun

Keywords:
Shale gas
Clay stabilizer
Kinetics
Isotherms
Adsorption
Desorption efficiency

ABSTRACT

Knowing methane desorption characteristics is essential to define the contribution of adsorbed gas to gas well production. To evaluate the synthetic effect of a clay stabilizer solution on methane desorption kinetics and isotherms pertaining to Longmaxi shale, an experimental setup was designed based on the volumetric method. The objective was to conduct experiments on methane adsorption and desorption kinetics and isotherms before and after clay stabilizer treatments. The experimental data were a good fit for both the intraparticle diffusion model and the Freundlich isotherm model. We analyzed the effect of the clay stabilizer on desorption kinetics and isotherms. Results show that clay stabilizer can obviously improve the diffusion rate constant and reduce the methane adsorption amount. Moreover, we analyzed the desorption efficiency before and after treatment as well as the adsorbed methane content. The results show that a higher desorption efficiency after treatment can be observed when the pressure is higher than 6.84 MPa. Meanwhile, the adsorbed methane content before and after treatment all increase when the pressure decreases, and clay stabilizer can obviously promote the adsorbed methane to free gas when the pressure is lower than 19 MPa. This can also be applied to the optimization formulation of slickwater and the design of gas well production.

1. Introduction

Unlike conventional or tight gas reservoirs, the natural gas in gas shale is mainly stored as a free gas phase and adsorbed gas phase, and the adsorbed gas phase accounts for 20%–85% of the original gas in place (Curtis, 2002), which is one potentially significant property impacting gas production over a long period of time (Rani et al., 2018; Loucks et al., 2009). Moreover, with the depletion of a gas reservoir, more adsorbed gas is translated into free gas, which not only provides more gas for production but also helps to sustain the free gas-phase pressure (Ambrose et al., 2010; Kuila and Prasad, 2013; Liu et al., 2021a). Thus, knowledge of methane desorption kinetics and isotherms is very important when addressing the role of shale gas desorption as being able to contribute significantly to production.

Methane desorption kinetics and isotherms on gas shale have been a hot research topic recently (Chai et al., 2019; Guo et al., 2020; Hu et al., 2020; Wu et al., 2015). Dasani et al. investigated the desorption behavior of pure methane (CH_4), ethane (C_2H_6), and their mixtures in a shale sample using thermogravimetric analysis (Dasani et al., 2017). Etminan et al. discussed the theory of gas adsorption-diffusion process through Fick's second law (Etminan et al., 2014). Wang et al. stated that the adsorption processing time extended linearly with the diameter of shale particle size (Wang et al., 2016a). Moreover, methane desorption isotherm in gas shale has been studied widely by gravimetric or volumetric isothermal methods (Guo et al., 2013; Rexer et al., 2013; Zhou et al., 2018). All the research results have demonstrated that methane desorption on shale is affected by the mineral constituents in shale rock (Heller and Zoback, 2014; Abdulkareem et al., 2020), total organic carbon (TOC) (Manger et al., 1991; Ross and Bustin, 2007), pore structure and micropore volume (Ross and Marc Bustin, 2009), kerogen type (Chalmers and Bustin, 2008), and temperature (Zhang et al., 2012).

At the same time, a few researchers have studied the effect of

* Corresponding author.
** Corresponding author.
E-mail addresses: baib@mst.edu (B.-J. Bai), wangyl@upc.edu.cn (Y.-L. Wang).

https://doi.org/10.1016/j.petsci.2021.09.025

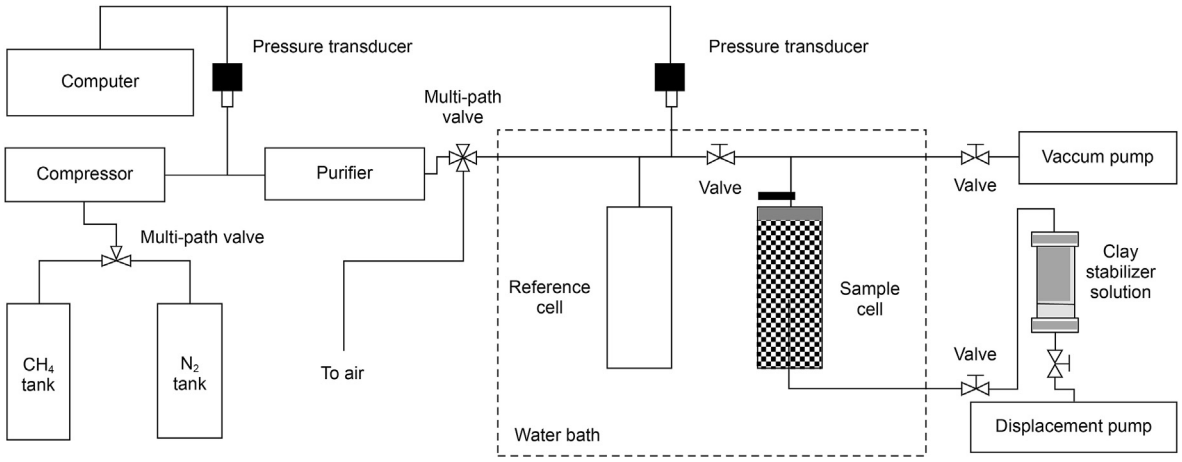

Fig. 1. Schematic representation of experimental setup.

slickwater and its chemical compositions on the petrophysical properties of shale (Hill et al., 2020; Liu et al., 2021b, 2021c, 2021d, 2021c; Siddiqui et al., 2019). Sun et al. studied the impact of surfactants on the imbibition mass in gas-saturated shale of the Marcellus shale in the Appalachian Basin of the eastern U.S. (Sun et al., 2015). Neog et al. demonstrated that a surfactant could alter the wettability of Wolfcamp shale (in western Texas, USA) to get a higher recovery (Neog and Schechter, 2016). Sun et al. reported that slickwater could significantly reduce the amount of methane adsorption on dry shale samples after slickwater treatment (Sun et al., 2018). All of this research was conducted on dry shale samples before and after chemicals solution treatments and the effect of the water in solution was not considered. However, the effect of the water in slickwater should not be neglected because it can occupy more than 99% of the total content (Sun et al., 2013; Wang et al., 2020). Additionally, the clay stabilizer is a major composition of slickwater, which is widely applied in gas shale reservoir stimulation and is known for its ability to inhibit clay swelling. Thus, it is very meaningful to evaluate the effect of clay stabilizer solution on methane desorption using a direct method.

The main purpose of this study is to investigate the clay stabilizer effect on methane desorption from Longmaxi shale samples considering the effect of the water in their solutions. The methane adsorption kinetics, desorption kinetics and isotherms before and after clay stabilizer treatments were conducted experimentally using volumetric method. We then analyzed the effect of the clay stabilizer on methane desorption kinetics, desorption isotherms, desorption efficiency and adsorbed methane content. These results can be very helpful for better understanding the function of clay stabilizer in slickwater, optimizing slickwater formula and designing of gas production.

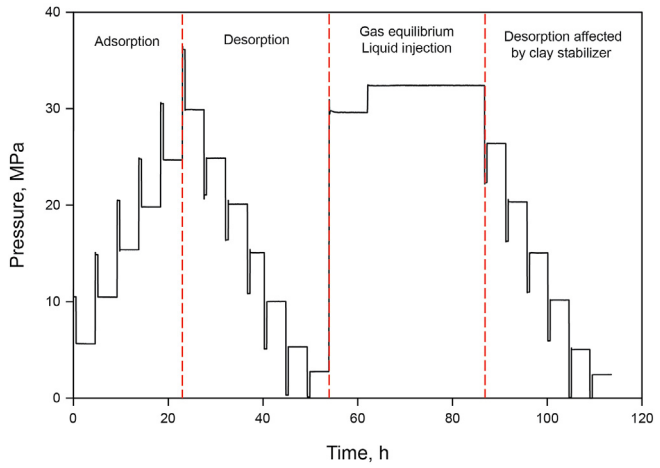

Fig. 2. Pressure response of multiple-step methane adsorption kinetic and isotherm experiment.

2. Experimental

2.1. Materials

The shale rocks in this study were obtained from a depth of about 1072 m of the Longmaxi gas shale formation in the northeast of the Sichuan Basin in Chongqing, China. The density of shale rock is 2.56 g/cm^3. Total organic carbon (TOC) content is 3.67 wt%. The primary minerals of shale sample are quartz, clay mineral, dolomite and plagioclase, and their contents are 47.4%, 31.6%, 9.1%, and 5.5%, respectively. The components of clay mineral in this sample are illite, cillite-smectite mixed layer and chlorite, and their contents are 70%, 25%, and 5%, respectively. The pore volume of micropores ($d \leq 2$ nm), mesopores ($2 < d \leq 50$ nm) and macropores ($d > 50$ nm) occupy 1.71%, 86.78%, and 11.51% of total pore volume, respectively. The rocks were crushed, and the shale powders with diameters between 0.25 and 0.125 mm were collected and dried in an oven at 60 °C for 48 h 130 g of samples was prepared for testing.

The clay stabilizer, as one of main compositions of slickwater, is a small molecule cationic amine hydrochloride. Its function is mainly to inhibit clay mineral swelling. Thus, 0.3 wt% of clay stabilizer solution was prepared with distilled water. Moreover, nitrogen (99.99 vol%) was used for testing void volume and checking for potential leaks in the experimental setup. Methane (99.99 vol%) was used as the adsorbate for conducting methane adsorption and desorption kinetic and isotherm experiments.

2.2. Experimental setup

The static volumetric method was used under constant temperature in this study for measuring methane adsorption and desorption kinetics and isotherms for shale powders. Specifically, the methane adsorption and desorption were tested based on mass balance equation, static gas balance and pressure measurement, and the adsorbed-phase and free-phase gas contents were calculated according to the changes of the pressure, volume and gas compressibility of the adsorbent before and after adsorption. This

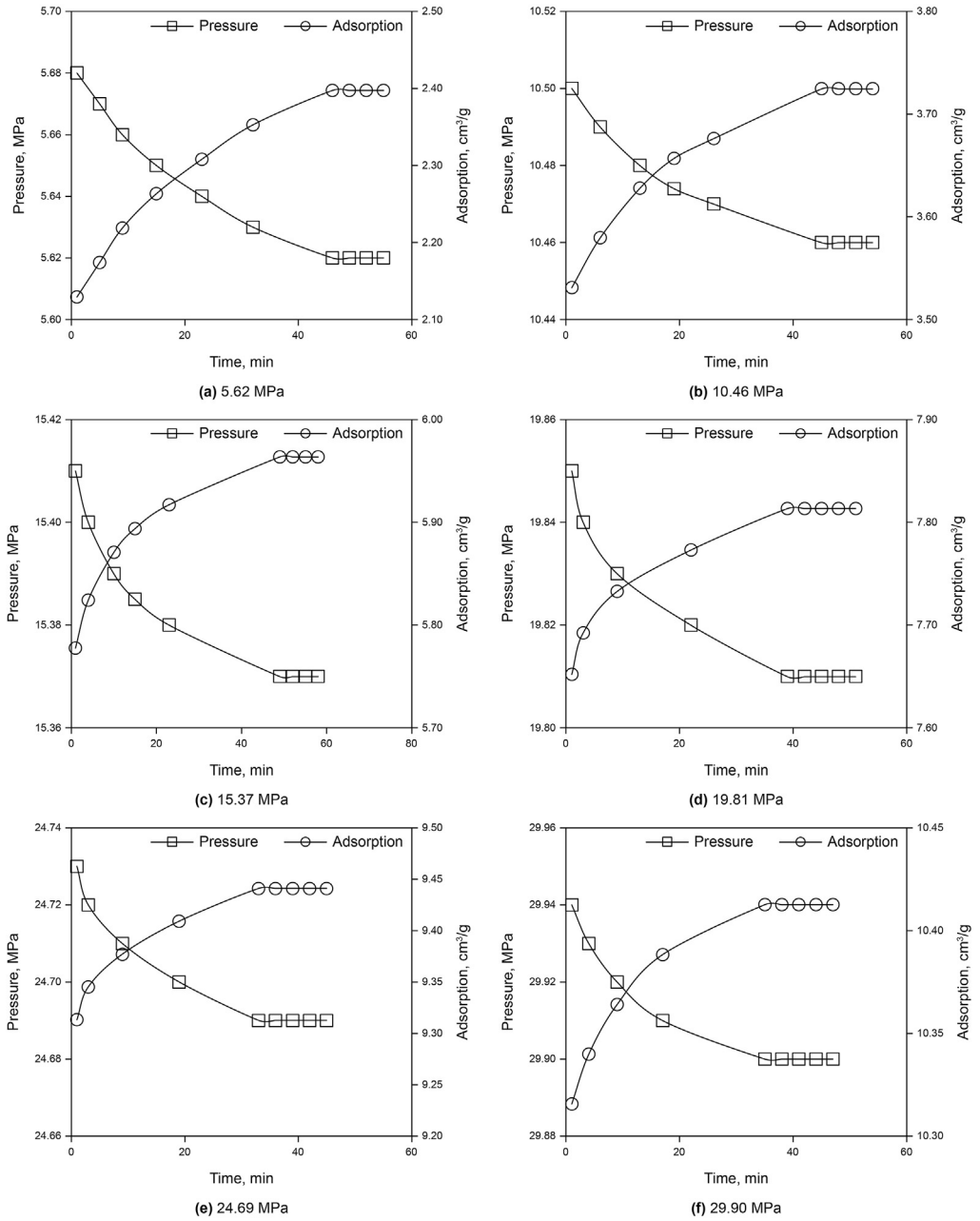

Fig. 3. Methane diffusion kinetics during the adsorption process.

method has been used successfully in previous studies (Chareonsuppanimit et al., 2012; Hall et al., 1994; Mohammad et al., 2009; Sudibandriyo et al., 2003). The schematic representation of the experimental setup is shown in Fig. 1. The reference cell and sample cell were maintained in a constant-temperature water bath. Nitrogen was applied to check for system leaks and to test the void volume in the sample cell. Methane was used for the adsorption and desorption tests on the shale powders. Pressure transducers were applied for reading the pressure during the adsorption and desorption progress, and the data were recorded in a computer. In the liquid injection system, a displacement pump was used to inject the clay stabilizer solution into the center of the powders in the sample cell.

2.3. Experimental procedure

To evaluate the clay stabilizer effect on the methane desorption kinetics and isotherms considering the process of liquid flowing into the samples as well as the function of huge-volume water, we focused on the role of clay stabilizer on methane desorption kinetics and isotherms at 30 °C. The procedure was implemented as follows:

(1) Preparation. After 130 g of shale powder with a diameter between 0.125 and 0.25 mm was placed into the sample cell, a filter screen was used to prevent powder from entering the valves. Then the sample was heated at 30 °C.
(2) Checking for system leaks. To assure the thermal equilibration of samples, nitrogen was used to check for system leaks

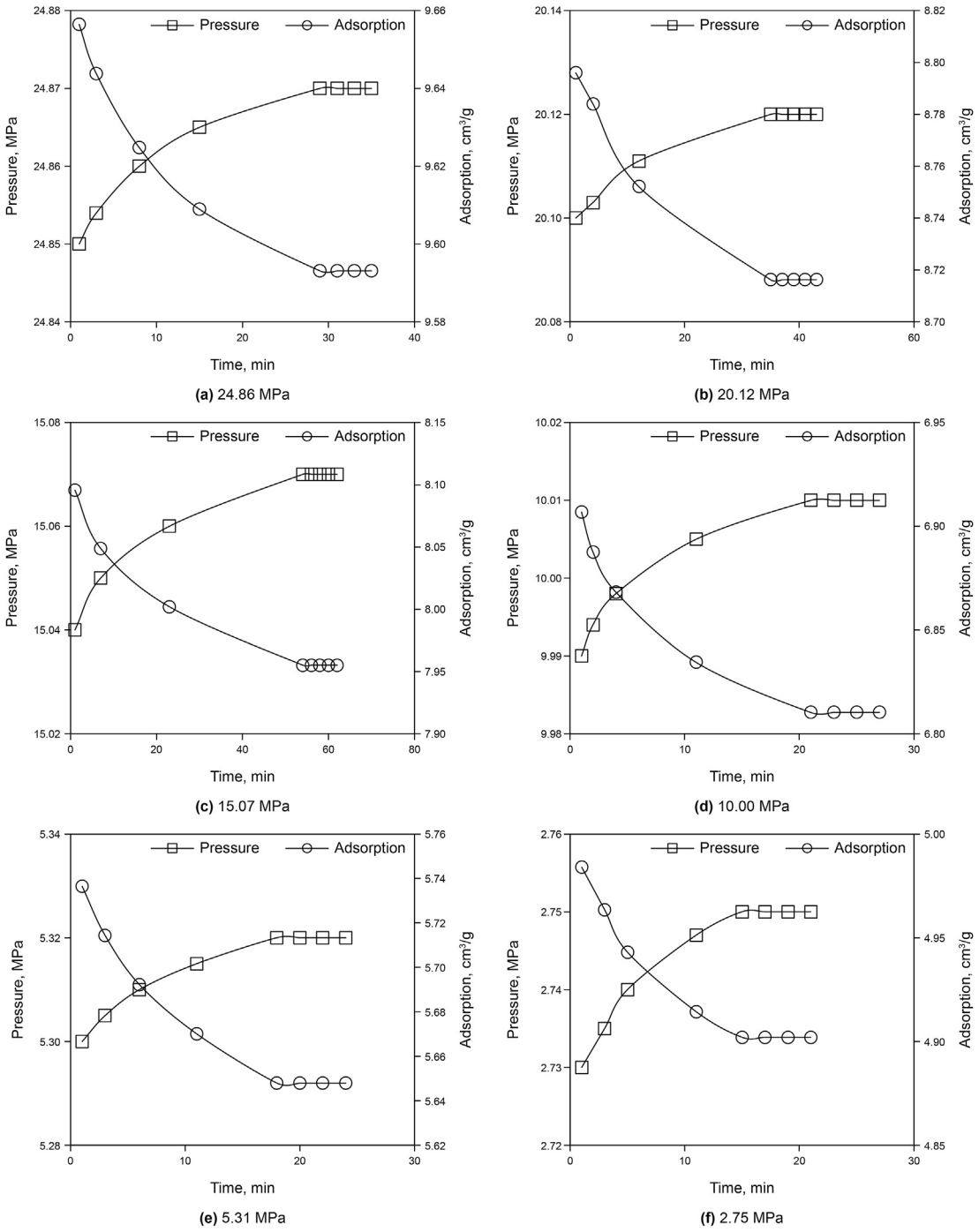

Fig. 4. Methane diffusion kinetics during the desorption process before it can be affected by the clay stabilizer.

at about 37 MPa and 30 °C, until the pressure was reached and kept constant for 2 h.

(3) Measuring void volume. The skeleton volume of shale powder in the sample cell was calculated based on Boyle's law by using equilibrium pressure data before and after nitrogen expanded four times. The void volume of the sample cell is equal to the difference between the sample cell volume and the skeleton volume of shale powder.

(4) Evacuating the vacuum reference cell and sample cell. The reference cell and sample cell were evacuated for 24 h by the vacuum pump. Then the valve between reference cell and sample cell was turned off.

(5) Measuring methane adsorption for kinetics and isotherms analysis. The reference cell was filled with methane. After equilibrium, the reference cell was connected to the sample cell. The pressure was read and stored before and after gas expansion. The amount of adsorbed gas was obtained at each stable pressure after the pressure was reached and kept constant. The methane adsorption kinetics and isotherms were obtained by repeating this step until the equilibrium pressure reached about 30 MPa.

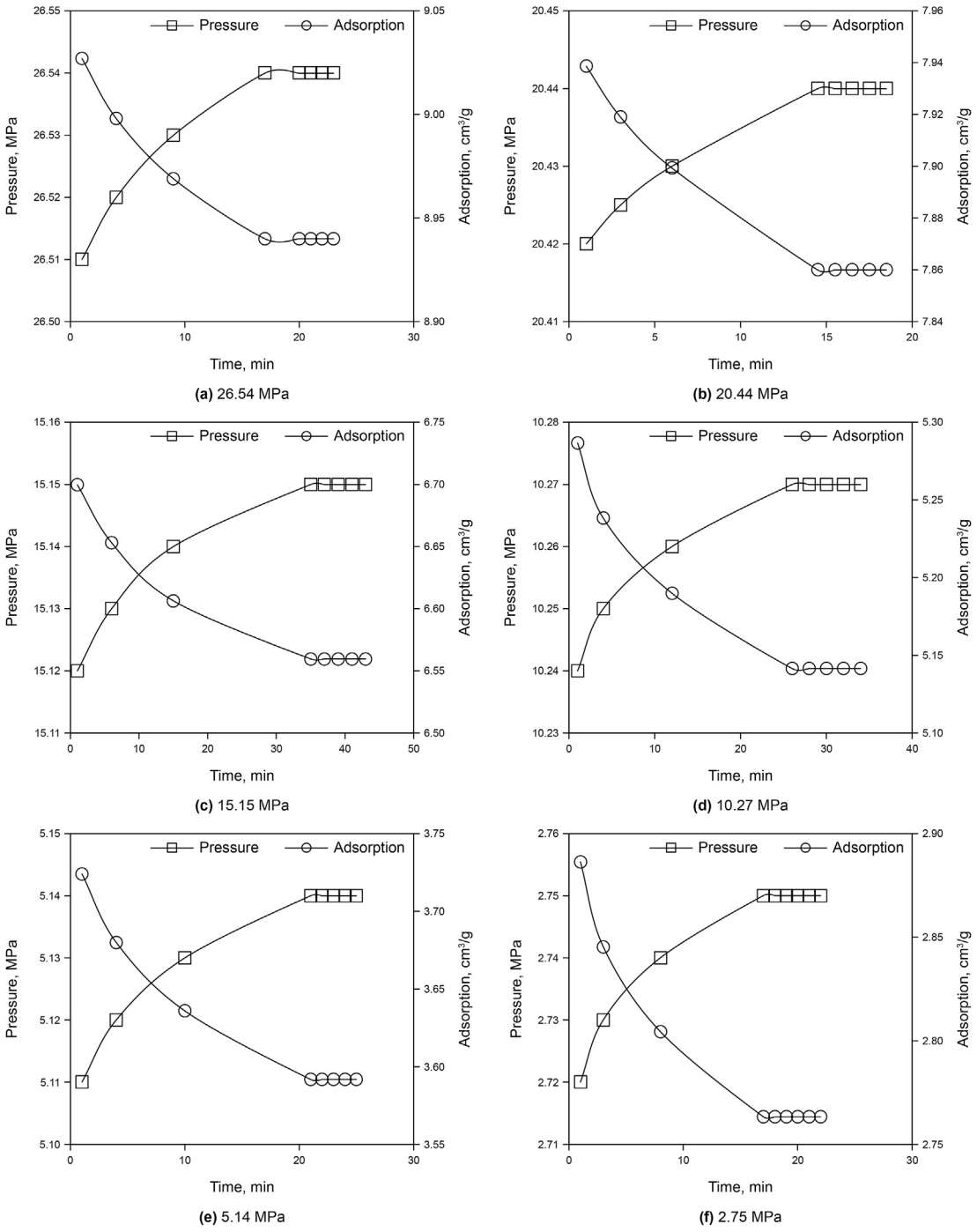

Fig. 5. Methane diffusion kinetics during the desorption process after being affected by the clay stabilizer.

(6) Measuring methane desorption kinetics and isotherms on dry shale powders. The valve between the reference cell and sample cell was turned off. Then the methane in the reference cell expanded to the outside of the experimental setup with a pressure drop of about 8 MPa. After equilibrium, the valve between reference cell and sample cell was connected. Repeat this step to the minimum pressure of about 3 MPa. The pressure response was read and recorded in a computer before and after expansion. The methane desorption kinetics and isotherms were produced.

(7) Measuring methane desorption kinetics and isotherms after the clay stabilizer treatment. The reference cell and sample cell were filled with methane again until the pressure was about 0.5 MPa above the maximum one in the process of measuring the methane adsorption kinetics and isotherms. After equilibrium, about 6 cm^3 of clay stabilizer solution was injected into the center of the sample cell by a displacement pump. The difference between the void volume tested by nitrogen and the volume of clay stabilizer solution injected by displacement pump was obtained to calculate the methane adsorption amount. After being maintained for

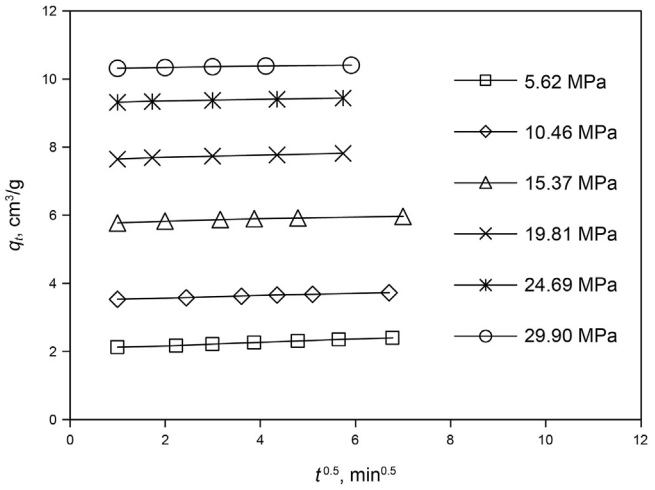

Fig. 6. Modeling methane adsorption kinetic during adsorption stage at six equilibrium pressures.

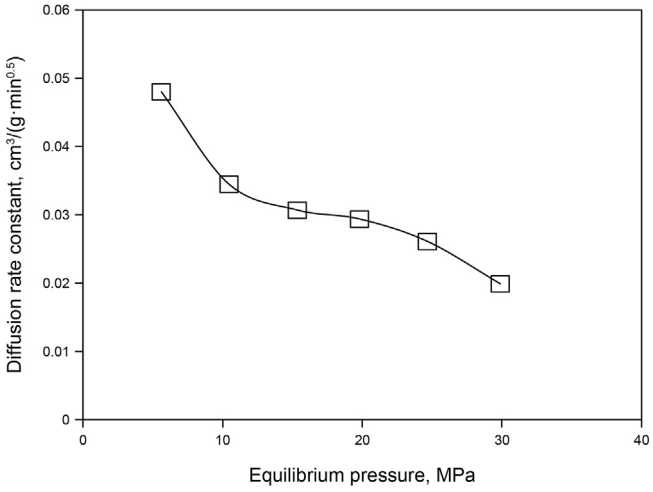

Fig. 7. The relationship between the diffusion rate constant and the equilibrium pressure.

24 h, the procedure continued by repeating the measurement of methane desorption kinetics and isotherms until the equilibrium pressure reduced to about 3 MPa.

3. Results and discussion

3.1. Experimental results

3.1.1. Pressure response curve characteristic of isothermal adsorption and desorption

Fig. 2 illustrates a volumetric method pressure response during multiple-step methane adsorption or desorption kinetics and isotherms on Longmaxi shale powder before and after the clay stabilizer treatment. The pressure curve can be divided into four stages: the adsorption stage, desorption stage, gas equilibrium and liquid injection stage, and the desorption stage after treatment. In the adsorption stage, there are six equilibrium-adsorption-equilibrium processes where the methane in the reference cell reached equilibrium in half an hour. Then, the methane expanded into shale powder in the sample cell, and the methane in both the reference cell and sample cell finally retained equilibrium again for each process. Furthermore, in the desorption stage, there are six equilibrium-desorption-equilibrium processes. Specifically, some methane was extracted from the reference cell after the valve between the reference cell and sample cell was turned off. Then, the valve was turned on again after the methane in the reference cell reached equilibrium. Finally, the methane in the reference cell and sample cell reached equilibrium again. After the methane was injected again into the reference cell and sample cell, it was maintained for 8 h to reach the equilibrium state. Then the clay stabilizer solution was displaced into the center of the shale powder in the sample cell and was kept there for 24 h. The last step consisted of measuring the methane desorption again as well as the pressure curve after the clay stabilizer treatment, which had a similar trend after the methane injection.

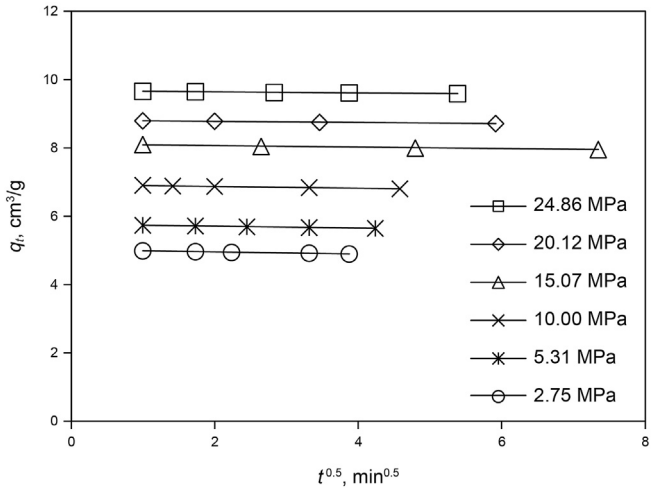

Fig. 8. Modeling methane desorption kinetics during desorption process at different equilibrium pressures.

3.1.2. Kinetic curve characteristic of methane adsorption and desorption

Figs. 3–5 present methane adsorption and desorption kinetics during the processes of adsorption and desorption before and after the clay stabilizer treatment, respectively. The tendency of the pressure curve during the methane adsorption stage quickly

Table 1
Modeling results of methane adsorption kinetics during the adsorption stage.

Equilibrium pressure, MPa	Fitting equation	R^2	Model	k
29.90	$y = 0.0199x + 10.300$	0.9825	$q_t = 0.0199t^{0.5} + 10.300$	0.0199
24.69	$y = 0.0261x + 9.2945$	0.9888	$q_t = 0.0261t^{0.5} + 9.2945$	0.0261
19.81	$y = 0.0294x + 7.6348$	0.9809	$q_t = 0.0294t^{0.5} + 7.6348$	0.0294
15.37	$y = 0.0307x + 5.7628$	0.9654	$q_t = 0.0307t^{0.5} + 5.7628$	0.0307
10.46	$y = 0.0345x + 3.4992$	0.9945	$q_t = 0.0345t^{0.5} + 3.4992$	0.0345
5.62	$y = 0.0480x + 2.0759$	0.9970	$q_t = 0.0480t^{0.5} + 2.0759$	0.0480

Table 2
Modeling results of methane desorption kinetics on dried shale sample.

Equilibrium pressure, MPa	Fitting equation	R^2	Model	k
24.86	$y = -0.0146x + 9.6688$	0.9877	$q_t = -0.0146t^{0.5} + 9.6688$	−0.0146
20.12	$y = -0.0167x + 8.8137$	0.9920	$q_t = -0.0167t^{0.5} + 8.8137$	−0.0167
15.07	$y = -0.0219x + 8.1117$	0.9909	$q_t = -0.0219t^{0.5} + 8.1117$	−0.0219
10.00	$y = -0.0263x + 6.9263$	0.9802	$q_t = -0.0263t^{0.5} + 6.9263$	−0.0263
5.31	$y = -0.0273x + 5.7619$	0.9966	$q_t = -0.0273t^{0.5} + 5.7619$	−0.0273
2.75	$y = -0.0290x + 5.0118$	0.9937	$q_t = -0.0290t^{0.5} + 5.0118$	−0.0290

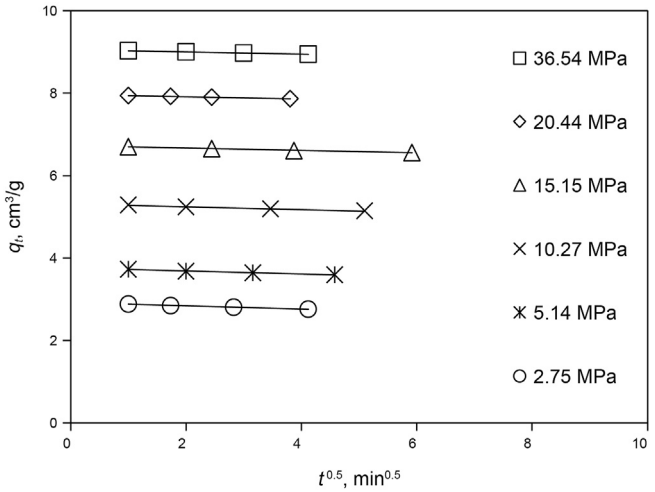

Fig. 9. Modeling methane desorption kinetics during the desorption stage after the clay stabilizer treatment at different equilibrium pressures.

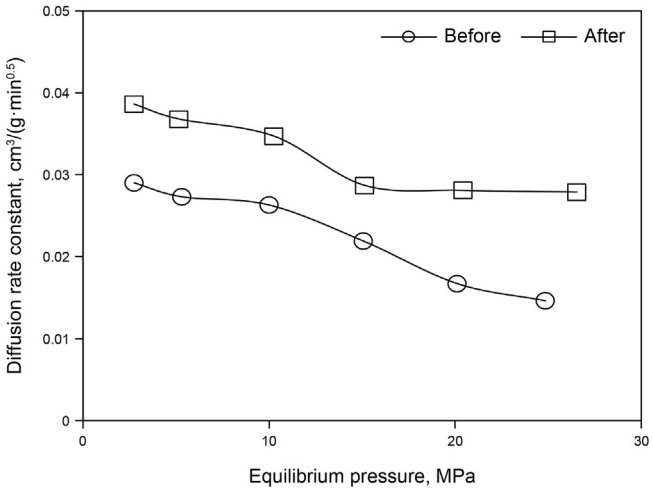

Fig. 10. The relationship between the diffusion rate constant and equilibrium pressure.

decrease at the beginning and then slowly stabilize at the end repeats itself. Meanwhile, the methane adsorption amount also increases quickly at first and then gradually slows down to finally maintain a constant. The two curves describing the methane adsorption kinetics follow the same tendency as in previous studies (Dasani et al., 2017; Chen et al., 2019). All the pressure curves during the desorption stages before and after the clay stabilizer treatment have the same tendency, indicating that pressure increases quickly at first and then gradually slows down before achieving stability at last. Moreover, the methane adsorption amount curves during desorption stages before and after the clay stabilizer treatment all have the same trend, which indicates that the methane adsorption amount decreases quickly at first; then it gradually slows down before finally retaining a constant.

3.2. Methane adsorption and desorption kinetic modeling

3.2.1. Intraparticle diffusion model

The intraparticle diffusion (IPD) model is widely applied for analyzing adsorption kinetics (Bai et al., 2009; Wu et al., 2009). The formula is expressed as follows:

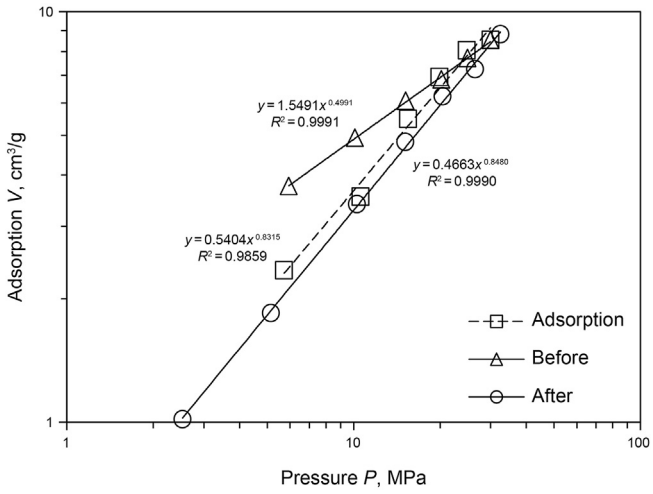

Fig. 11. Modeling the methane adsorption isotherm and the desorption isotherm before and after the clay stabilizer treatment.

Table 3
Modeling results of methane desorption kinetics during desorption process after treatment.

Equilibrium pressures, MPa	Fitting equations	R^2	Model	k
26.54	$y = -0.0279x + 9.0542$	0.9991	$q_t = -0.0279t^{0.5} + 9.0542$	−0.0279
20.44	$y = -0.0281x + 7.9673$	0.9996	$q_t = -0.0281t^{0.5} + 7.9673$	−0.0281
15.15	$y = -0.0287x + 6.7245$	0.9917	$q_t = -0.0287t^{0.5} + 6.7245$	−0.0287
10.27	$y = -0.0347x + 5.3145$	0.9890	$q_t = -0.0347t^{0.5} + 5.3145$	−0.0347
5.14	$y = -0.0368x + 3.7566$	0.9938	$q_t = -0.0368t^{0.5} + 3.7566$	−0.0368
2.75	$y = -0.0386x + 2.9182$	0.9855	$q_t = -0.0386t^{0.5} + 2.9182$	−0.0386

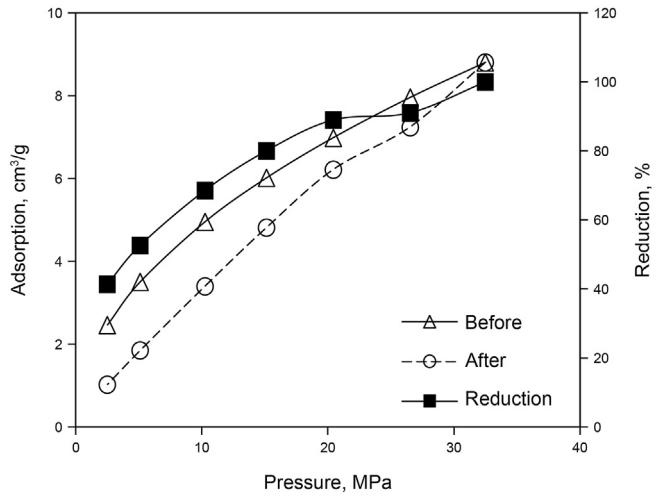

Fig. 12. The desorption isotherm versus pressure before and after the clay stabilizer treatment.

$$q_t = kt^{1/2} + C \quad (1)$$

where q_t is the methane adsorption amount in cm^3/g, k is the diffusion rate constant in $cm^3/(g \cdot min^{1/2})$, C is a constant. The plot of q_t versus $t^{1/2}$ should fit as a straight line, and k and C can be calculated according to the slope and the y-intercept. Thus, q_t can be calculated according to k, C and t.

3.2.2. Adsorption kinetic modeling

We applied the IPD model to determine the methane adsorption kinetics on shale by using Eq (1). Fig. 6 illustrates that q_t as the y axis is a linear fitting relationship with $t^{1/2}$ as the x axis for six different pressure points of 29.90, 24.69, 19.81, 15.37, 10.46, and 5.62 MPa. Table 1 lists the fitting equation, correlation coefficient, model, and diffusion rate constant. It is obvious that the methane adsorption amount is well fitted as a straight line with $t^{1/2}$ because the correlation coefficients range between 0.9825 and 0.9970. The diffusion rate constant distributes from 0.0199 to 0.0480 $cm^3/(g \cdot min^{1/2})$, and it decreases with the increase in equilibrium pressure, as shown in Fig. 7.

3.2.3. Desorption kinetic modeling

The IPD model was also used for describing methane desorption kinetics by using Eq. (1). Fig. 8 shows the methane adsorption amount decreasing as a linear function of the square root of time at the pressures of 24.86, 20.12, 15.07, 10.00, 5.31, and 2.75 MPa. The fitting equation, correlation coefficient, model and diffusion rate constant are listed in Table 2. Clearly, the methane adsorption amount has a good straight line relationship with the square root of time because all the correlation coefficients are higher than 0.9802. Parameter k distributes from −0.0146 to −0.0290.

3.2.4. Desorption kinetic modeling after clay stabilizer treatment

The IPD model is applied to fit the methane desorption kinetic data during the desorption stage after the clay stabilizer treatment by using Eq. (1). The linear relationship between q_t and $t^{0.5}$ is depicted in Fig. 9 at the pressures of 36.54, 20.44, 15.15, 10.27, 5.14 and 2.75 MPa. Table 3 lists the modeling results by showing the fitting equations, correlation coefficients, models and diffusion rate constants. It can be seen that q_t has a good linear relationship with $t^{0.5}$ because all the correlation coefficients are greater than 0.9890. Parameter k distributes from −0.0279 to −0.0386.

3.3. The effect of clay stabilizer on methane desorption kinetics

After fitting the relationship between q_t and $t^{0.5}$, we found that parameter k during the methane desorption stage before and after the clay stabilizer treatment is less than zero. We define the absolute value of constant k as the diffusion rate constant during the methane desorption stage. Fig. 10 shows the plot of the diffusion rate constant versus the equilibrium pressure before and after the clay stabilizer treatment. The diffusion rate constant before the clay stabilizer treatment decreases as the approximate linear relationship with equilibrium pressure. Moreover, the diffusion rate constant after the clay stabilizer treatment decreases approximate linearly until the equilibrium pressure reaches 15.15 MPa, and it remains stable when the pressure is bigger than 15.15 MPa. Moreover, the diffusion rate constant after the clay stabilizer treatment is significantly bigger than that before the treatment, indicating that clay stabilizer can obviously improve the diffusion rate constant, and even promote methane to reach the bottom of well with more quick speed. That is to say clay stabilizer solution retaining in shale gas reservoir can increase the shale-gas well

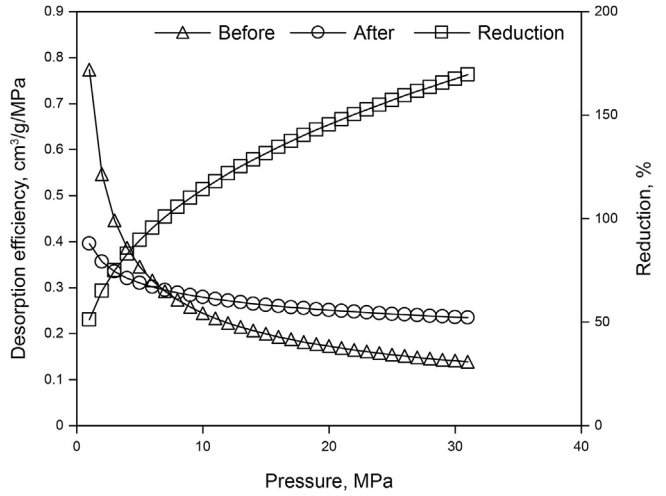

Fig. 13. Desorption efficiency versus the pressure and desorption efficiency reduction versus pressure before and after the clay stabilizer treatment.

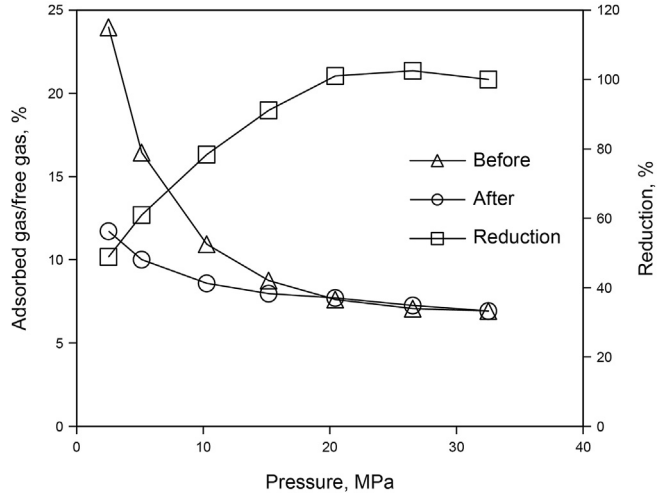

Fig. 14. The ratio of adsorbed gas to free gas versus equilibrium pressure before and after clay stabilizer treatment.

production.

3.4. The effect of the clay stabilizer on the desorption isotherm

3.4.1. The Freundlich isotherm model

The excess adsorption amount can be calculated through the pressure response data based on volumetric method. Moreover, the excess adsorption amount can be converted to absolute adsorption amount using the following equation (Chen et al., 2019; Gasparik et al., 2012; Krooss et al., 2002):

$$n_{abs} = \frac{n_{exc}}{1 - \rho_{gas}/\rho_{ads}} \tag{2}$$

where n_{abs} is the absolute adsorption amount in cm^3/g; n_{exc} is the excess adsorption amount in cm^3/g; ρ_{gas} is the density of the free gas phase in g/cm^3, and ρ_{ads} is the density of the adsorbed gas phase in g/cm^3. The adsorbed methane density of 0.548 g/cm^3 is calculated by Thomas et al. (Rexer et al., 2013) using the supercritical Dubinin−Radushkevich model at 303.15 K, and this value is applied in this work.

The Freundlich isotherm model is an empirical formula for describing adsorption and desorption characteristics on a heterogeneous surface. The equation is expressed as (Wang et al., 2016b; Dada et al., 2012):

$$V = kP^n \tag{3}$$

where V is the methane adsorption amount per unit of mass shale powder in cm^3/g; P is the equilibrium pressure in MPa; k is the Freundlich constant representing adsorption capacity; and n is a constant.

3.4.2. Freundlich isotherm modeling

The relationship between V and P during the adsorption stage and desorption stage before and after the clay stabilizer treatment can be fitted on the log-log scale plot as shown in Fig. 11 by using Eq. (3), and the models can be expressed as follows:

$$\text{Adsorption } V = 0.5404P^{0.8315},\ R^2 = 0.9859 \tag{4}$$

$$\text{Desorption before treatment } V = 1.5491\text{P}^{0.4991},\ R^2 = 0.9991 \tag{5}$$

$$\text{Desorption after treatment } V = 0.4663P^{0.8480},\ R^2 = 0.9990 \tag{6}$$

Clearly, the methane adsorption amount and equilibrium pressure can be well fitted by using the Freundlich isotherm model, because the correlation coefficients (R^2) are all greater than 0.99. Furthermore, the adsorption capacities of the adsorption and desorption isotherm on dry shale samples are 0.5404 and 1.5491, respectively, indicating there exists an obvious hysteresis phenomenon in the adsorption capacity between adsorption and desorption isotherms. Meanwhile, the adsorption capacity of the desorption isotherms before and after clay stabilizer treatments are 1.5491 and 0.4663, respectively. Moreover, the methane adsorption amounts are calculated by using Eq. (5) at six equilibrium pressures, which are the same as that found in the desorption process after the clay stabilizer treatment. The comparison plot of the desorption isotherm before and after the clay stabilizer treatment is shown in Fig. 12. Clearly, the methane adsorption amount after the clay stabilizer treatment is substantially less than before, and the ratio of the adsorption amount after the treatment compared to that before the treatment reduces as the equilibrium pressure decreases. Therefore, the clay stabilizer can obviously reduce the methane adsorption capacity on shale powders.

3.5. The effect of the clay stabilizer on desorption efficiency

Desorption efficiency is defined as the desorbed amount of the shale gas under the unit pressure drop to quantitatively characterize the desorbed quantity and desorbed rate. In this study, desorption efficiency (η) can be expressed by the first derivative of the Freundlich isotherm equation as follows (Liu et al., 2020, 2021c):

$$\eta = V' = knP^{n-1} \tag{7}$$

Thus, desorption efficiency is calculated by using Eq. (7) after modeling the Freundlich isotherm.

According to the expression of desorption efficiency as shown in Eq. (7), the first derivatives of the Freundlich isotherm model before and after the clay stabilizer treatment are obtained by using Eqs. (5) and (6) as follows:

$$\text{Before}: \ \eta = V' = 0.7732 \cdot P^{-0.5009} \tag{8}$$

$$\text{After}: \eta = V' = 0.3954 \cdot P^{-0.1520} \tag{9}$$

Then, the desorption efficiency before and after the clay stabilizer treatment and desorption efficiency reduction are plotted in Fig. 13. Here, the two desorption efficiency curves all increase while equilibrium pressure decreases. The two curves have an intersection point. Before this intersection point, the desorption efficiency before the clay stabilizer treatment is obviously greater than that after, and the desorption efficiency reduction is less than 100%; meanwhile, after this point, the desorption efficiency before the clay stabilizer treatment is obviously smaller than that after, and the desorption efficiency reduction is more than 100%. Thus, in this paper, we can define this point as the desorption equivalent point. When Eq. (8) is equal to Eq. (9), the pressure of desorption equivalent point can be calculated as 6.84 MPa and the desorption efficiency at this point is 0.30 $cm^3/g/MPa$. Therefore, the higher desorption efficiency after the clay stabilizer treatment can be obtained when the pressure is more than 6.84 MPa, and the desorption efficiency reduction increases as the pressure increases. This can also guide the optimization of the flowing bottom hole pressure of a gas well after hydraulic fracturing.

3.6. The effect of the clay stabilizer on adsorbed methane content

Adsorbed methane in a shale reservoir has an obvious effect on gas well production (Wang et al., 2017; Mengal and Wattenbarger, 2011). In this study, we define the ratio of adsorbed gas to free gas as adsorbed methane content, which is used to analyze the influence of the clay stabilizer on the adsorbed methane content. The ratio before and after the clay stabilizer treatment and the ratio reduction are plotted in Fig. 14. Here, the ratio before clay stabilizer treatment decreases quickly at first; then, it gradually decreases. The ratio after the clay stabilizer treatment gradually decreases from the beginning, which is a little higher than that before treatment when the equilibrium pressure reaches about 19 MPa. Meanwhile, the reduction of the ratio after the clay stabilizer treatment to the ratio before the treatment increases quickly at first, but then remains constant when the equilibrium pressure reaches about 19 MPa. Therefore, the adsorbed methane ratio before and after the clay stabilizer treatment increases with the decrease in pressure, and the clay stabilizer can obviously promote the adsorbed methane translate into the free gas phase when the pressure is smaller than 19 MPa.

4. Conclusions

Adsorption kinetics of the methane adsorption and desorption on the Longmaxi shale powder before and after the clay stabilizer treatment all fit the intraparticle diffusion model very well. The clay stabilizer can increase the diffusion rate constant during methane desorption.

Methane adsorption and desorption isotherms on Longmaxi shale before and after clay stabilizer treatment are all well fitted with the Freundlich model. An obvious hysteresis phenomenon exists in its adsorption capacity curves between adsorption and desorption isotherms. The clay stabilizer can significantly reduce methane adsorption amounts during methane desorption.

The desorption efficiency of methane on shale powder can be substantially affected by the clay stabilizer. The clay stabilizer can reduce the desorption efficiency when the pressure is less than 6.84 MPa. Conversely, the stabilizer can increase the desorption efficiency when the pressure is bigger than 6.84 MPa.

The adsorbed methane ratio before and after the clay stabilizer treatment increases with the decrease of pressure, and the clay stabilizer can obviously promote the adsorbed methane transported into the free gas phase when the pressure is smaller than 19 MPa.

Acknowledgements

First author, Zhong-Hua Liu expresses sincere appreciation to the Missouri University of Science and Technology for providing the opportunity to serve as a visiting scholar. This research is supported by the China Scholarship Council (No.201908505143), the Chongqing Research Program of Basic Research and Frontier Technology (No.cstc2017jcyjAX0290/No.cstc2018jcyjAX0563).

References

Abdulkareem, F.A., Radman, A., Faugere, G., Sathiavelu, S., Irfan, S.A., Padmanabhan, E., 2020. Petro-physical properties of Marcellus shale samples and their impact on CO_2 adsorption: equilibrium, kinetics, and empirical modeling study. J. Nat. Gas Sci. Eng. 81, 103423. https://doi.org/10.1016/j.jngse.2020.103423.

Ambrose, R.J., Hartman, R.C., Diaz-Campos, M., Akkutlu, I.Y., Sondergeld, C.H., 2010. New pore-scale considerations for shale gas in place calculations. SPE Unconventional Gas Conference. https://doi.org/10.2523/131772-MS.

Bai, B., Wu, Y., Grigg, R.B., 2009. Adsorption and desorption kinetics and equilibrium of calcium lignosulfonate on dolomite porous media. J. Phys. Chem. C 113 (31), 13772–13779. https://doi.org/10.1021/jp9028326.

Chai, D., Yang, G., Fan, Z., Li, X., 2019. Gas transport in shale matrix coupling multilayer adsorption and pore confinement effect. Chem. Eng. J. 370 (15), 1534–1549. https://doi.org/10.1016/j.cej.2019.03.276.

Chalmers, G.R.L., Bustin, R.M., 2008. Lower Cretaceous gas shales in northeastern British Columbia, Part I: geological controls on methane sorption capacity. Bull. Can. Petrol. Geol. 56 (1), 1–21. https://doi.org/10.2113/gscpgbull.56.1.1.

Chareonsuppanimit, P., Mohammad, S.A., Robinson, R.L., Gasem, K.A.M., 2012. High-pressure adsorption of gases on shales: measurements and modeling. Int. J. Coal Geol. 95 (1), 34–46. https://doi.org/10.1016/j.coal.2012.02.005.

Chen, L., Zuo, L., Jiang, Z., Jiang, S., Liu, K., Tan, J., et al., 2019. Mechanisms of shale gas adsorption: evidence from thermodynamics and kinetics study of methane adsorption on shale. Chem. Eng. J. 361 (1), 559–570. https://doi.org/10.1016/j.cej.2018.11.185.

Curtis, J.B., 2002. Fractured shale-gas systems. AAPG (Am. Assoc. Pet. Geol.) Bull. 86 (11), 1921–1938. https://doi.org/10.1306/61EEDDBE-173E-11D7-8645000102C1865D.

Dada, A.O., Olalekan, A.P., Olatunya, A.M., Dada, O., 2012. Langmuir, Freundlich, Temkin and Dubinin–Radushkevich isotherms studies of equilibrium sorption of Zn^{2+} unto phosphoric acid modified rice husk. IOSR J. Appl. Chem. 3 (1), 38–45. https://doi.org/10.9790/5736-0313845.

Dasani, D., Wang, Y., Tsotsis, T.T., Jessen, K., 2017. Laboratory-scale investigation of sorption kinetics of methane/ethane mixtures in shale. Ind. Eng. Chem. Res. 56 (36), 9953–9963. https://doi.org/10.1021/acs.iecr.7b02431.

Etminan, S.R., Javadpour, F., Maini, B.B., Chen, Z., 2014. Measurement of gas storage processes in shale and of the molecular diffusion coefficient in kerogen. Int. J. Coal Geol. 123 (1), 10–19. https://doi.org/10.1016/j.coal.2013.10.007.

Gasparik, M., Ghanizadeh, A., Bertier, P., Gensterblum, Y., Bouw, S., Krooss, B.M., 2012. High-pressure methane sorption isotherms of black shales from The Netherlands. Energy Fuels 26 (8), 4995–5004. https://doi.org/10.1021/ef300405g.

Guo, C., Li, R., Sun, J., Wang, X., Liu, H., 2020. A review of gas transport and adsorption mechanisms in two-component methane-carbon dioxide system. Int. J. Energy Res. 44 (4), 2499–2516. https://doi.org/10.1002/er.5114.

Guo, W., Xiong, W., Gao, S., Hu, Z., Liu, H., Yu, R., 2013. Impact of temperature on the isothermal adsorption/desorption of shale gas. Petrol. Explor. Dev. 40 (4), 514–519. https://doi.org/10.1016/S1876-3804(13)60066-X.

Hall, F.E., Zhou, C., Gasem, K.A.M., Robinson, R.L., Yee, D., 1994. Adsorption of Pure Methane, Nitrogen, and Carbon Dioxide and Their Binary Mixtures on Wet Fruitland Coal. SPE Eastern Regional Meeting. https://doi.org/10.2118/29194-MS.

Heller, R., Zoback, M., 2014. Adsorption of methane and carbon dioxide on gas shale and pure mineral samples. J. Unconv. Oil Gas Resour. 8 (C), 14–24. https://doi.org/10.1016/j.juogr.2014.06.001.

Hill, A., Zhu, D., Moridis, G., Correa, J., Zoback, M., Ajo-Franklin, J., et al., 2020. The Eagle Ford shale laboratory: a field study of the stimulated reservoir volume, detailed fracture characteristics, and EOR potential. In: PE/AAPG/SEG Unconventional Resources Technology Conference. https://doi.org/10.15530/urtec-2020-2973.

Hu, A., Zhang, Y., Xiong, P., Yang, Y., Liu, Z., 2020. Kinetic characteristics and modeling comparison of methane adsorption on gas shale. Energy Sources, Part A Recover. Util. Environ. Eff. https://doi.org/10.1080/15567036.2020.1849461.

Krooss, B.M., van Bergen, F., Gensterblum, Y., Siemons, N., Pagnier, H.J.M., David, P., 2002. High-pressure methane and carbon dioxide adsorption on dry and moisture-equilibrated Pennsylvanian coals. Int. J. Coal Geol. 51 (2), 69–92. https://doi.org/10.1016/S0166-5162(02)00078-2.

Kuila, U., Prasad, M., 2013. Specific surface area and pore-size distribution in clays and shales. Geophys. Prospect. 61 (2), 341–362. https://doi.org/10.1111/1365-2478.12028.

Liu, Z., Bai, B., Wang, Y., Ding, Z., Li, J., Qu, H., et al., 2020. Experimental study of friction reducer effect on dynamic and isotherm of methane desorption on Longmaxi shale. Fuel 288 (15). https://doi.org/10.1016/j.fuel.2020.119733.

Liu, Z., Bai, B., Ding, Z., Qu, H., Zeng, S., Da, X., 2021a. Impact of cleanup additive on methane desorption on Longmaxi shale. Fuel 300 (15). https://doi.org/10.1016/j.fuel.2021.121003.

Liu, Z., Bai, B., Tang, J., Xiang, Z., Zeng, S., Qu, H., 2021b. Investigation of slickwater effect on permeability of gas shale from longmaxi formation. Energy Fuels 35 (4), 3104–3111. https://doi.org/10.1021/acs.energyfuels.0c04081.

Liu, Z., Bai, B., Wang, Y., Qu, H., Ding, Z., Xiao, Q., 2021c. Experimental study of slickwater volume effect on methane desorption on Longmaxi shale. J. Nat. Gas Sci. Eng. 91. https://doi.org/10.1016/j.jngse.2021.103950.

Liu, Z., Bai, B., Wang, Y., Qu, H., Xiao, Q., Zeng, S., 2021d. Spontaneous imbibition characteristics of slickwater and its components in Longmaxi shale. J. Petrol. Sci. Eng. 202. https://doi.org/10.1016/j.petrol.2021.108599.

Loucks, R.G., Reed, R.M., Ruppel, S.C., Jarvie, D.M., 2009. Morphology, genesis, and distribution of nanometer-scale pores in siliceous mudstones of the mississippian barnett shale. J. Sediment. Res. 79 (12), 848–861. https://doi.org/10.2110/jsr.2009.092.

Manger, K.C., Oliver, S.J.P., Curtis, J.B., Scheper, R.J., 1991. Geologic Influences on the Location and Production of Antrim Shale Gas, Michigan Basin. Low Permeability Reservoirs Symposium. https://doi.org/10.2523/21854-MS.

Mengal, S.A., Wattenbarger, R.A., 2011. Accounting for adsorbed gas in Shale gas reservoirs. SPE Middle East Oil and Gas Show and Conference. https://doi.org/10.2118/141085-MS.

Mohammad, S.A., Chen, J.S., Fitzgerald, J.E., Robinson, R.L., Gasem, K.A.M., 2009. Adsorption of pure carbon dioxide on wet argonne coals at 328.2 K and pressures up to 13.8 MPa. Energy Fuels 23 (2), 1107–1117. https://doi.org/10.1021/ef800870a.

Neog, A., Schechter, D.S., 2016. Investigation of surfactant induced wettability alteration in Wolfcamp shale for hydraulic fracturing and EOR applications. In: SPE Improved Oil Recovery Conference. https://doi.org/10.2118/179600-MS.

Rani, S., Prusty, B.K., Pal, S.K., 2018. Adsorption kinetics and diffusion modeling of CH_4 and CO_2 in Indian shales. Fuel 216, 61–70. https://doi.org/10.1016/j.fuel.2017.11.124.

Rexer, T.F.T., Benham, M.J., Aplin, A.C., Thomas, K.M., 2013. Methane adsorption on shale under simulated geological temperature and pressure conditions. Energy Fuels 27 (6), 3099–3109. https://doi.org/10.1021/ef400381v.

Ross, D.J.K., Bustin, R.M., 2007. Shale gas potential of the lower jurassic Gordondale member, northeastern British Columbia, Canada. Bull. Can. Petrol. Geol. 55 (1), 51–75. https://doi.org/10.2113/gscpgbull.55.1.51.

Ross, D.J.K., Marc Bustin, R., 2009. The importance of shale composition and pore structure upon gas storage potential of shale gas reservoirs. Mar. Petrol. Geol. 26 (6), 916–927. https://doi.org/10.1016/j.marpetgeo.2008.06.004.

Siddiqui, M.A.Q., Chen, X., Iglauer, S., Roshan, H., 2019. A multiscale study on shale wettability: spontaneous imbibition versus contact angle. Water Resour. Res. 55 (6), 5012–5032. https://doi.org/10.1029/2019WR024893.

Sudibandriyo, M., Pan, Z., Fitzgerald, J.E., Robinson, R.L., Gasem, K.A.M., 2003. Adsorption of methane, nitrogen, carbon dioxide, and their binary mixtures on dry activated carbon at 318.2 K and pressures up to 13.6 MPa. Langmuir 84 (18), 2351–2363. https://doi.org/10.1021/la020976k.

Sun, Y., Zhang, H., Wu, Q., Wei, M., Bai, B., Ma, Y., 2013. Experimental study of friction reducer flows in microfracture during slickwater fracturing. In: SPE International Symposium on Oilfield Chemistry. https://doi.org/10.2118/164053-MS.

Sun, Y., Bai, B., Wei, M., 2015. Microfracture and surfactant impact on linear cocurrent brine imbibition in gas-saturated shale. Energy Fuels 29 (3), 1438–1446. https://doi.org/10.1021/ef5025559.

Sun, Z., Zhang, H., Wei, Z., Wang, Y., Wu, B., Zhuo, S., et al., 2018. Effects of slick water fracturing fluid on pore structure and adsorption characteristics of shale reservoir rocks. J. Nat. Gas Sci. Eng. 51, 27–36. https://doi.org/10.1016/j.jngse.2017.12.030.

Wang, J., Wang, B., Li, Y., Yang, Z., Gong, H., Dong, M., 2016a. Measurement of dynamic adsorption-diffusion process of methane in shale. Fuel 172, 37–48.

Wang, J., Dong, M., Yang, Z., Gong, H., Li, Y., 2017. Investigation of methane desorption and its effect on the gas production process from shale: experimental and mathematical study. Energy Fuels 31 (1), 205–216. https://doi.org/10.1016/j.petrol.2020.107359, 10.1021/acs.energyfuels.6b02033.

Wang, J., Zhou, F., Bai, H., Li, Y., Yang, H., 2020. A comprehensive method to evaluate the viscous slickwater as fracturing fluids for hydraulic fracturing applications. J. Petrol. Sci. Eng. 193. https://doi.org/10.1016/j.fuel.2015.12.069.

Wang, Z., Li, Y., Guo, P., Meng, W., 2016b. Analyzing the adaption of different adsorption models for describing the shale gas adsorption law. Chem. Eng. Technol. 39 (10), 1921–1932. https://doi.org/10.1002/ceat.201500617.

Wu, F.C., Tseng, R.L., Juang, R.S., 2009. Initial behavior of intraparticle diffusion model used in the description of adsorption kinetics. Chem. Eng. J. 153 (1), 1–8. https://doi.org/10.1016/j.cej.2009.04.042.

Wu, K., Li, X., Wang, C., Yu, W., Chen, Z., 2015. Model for surface diffusion of adsorbed gas in nanopores of shale gas reservoirs. Ind. Eng. Chem. Res. 54 (12). https://doi.org/10.1021/ie504030v.

Zhang, T., Ellis, G.S., Ruppel, S.C., Milliken, K., Yang, R., 2012. Effect of organic-matter type and thermal maturity on methane adsorption in shale-gas systems. Org. Geochem. 47, 120–131. https://doi.org/10.1016/j.orggeochem.2012.03.012.

Zhou, S., Xue, H., Ning, Y., Guo, W., Zhang, Q., 2018. Experimental study of supercritical methane adsorption in Longmaxi shale: insights into the density of adsorbed methane. Fuel 211, 140–1488. https://doi.org/10.1016/j.fuel.2017.09.065.